Available online at www.sciencedirect.com
ScienceDirect
Trans. Nonferrous Met. Soc. China 33(2023) 1205−1213
Transactions of Nonferrous Metals Society of China
www.tnmsc.cn

Synthesis and up-conversion luminescence of Ho^{3+} and Yb^{3+} co-doped $La_7P_3O_{18}$ phosphors

Hao-tian ZHU[1], Hai-rui GUO[1], Qi-jing ZHENG[1], Chun-yan GUAN[1], Li-ping ZHU[2], Hai-bin LI[3], Jin-yu YANG[1]

1. Key Laboratory for Functional Materials Chemistry of Guizhou Province, School of Chemistry and Materials Science, Guizhou Normal University, Guiyang 550001, China;
2. Institute of Education, Guizhou Normal University, Guiyang 550001, China;
3. Guangxi Key Laboratory of Agricultural Resources Chemistry and Biotechnology, College of Chemistry and Food Science, Yulin Normal University, Yulin 537000, China

Received 11 November 2021; accepted 30 March 2022

Abstract: Ho^{3+} and Yb^{3+} co-doped $La_7P_3O_{18}$ up-conversion phosphors were prepared by a high-temperature solid-state process. XRD results reveal that the samples are mixtures of monoclinic structure $La_7P_3O_{18}$ crystals with $P21/n$ space group and minor $LaPO_4$ crystals. UV−Vis DRS results indicate that $La_7P_3O_{18}$ crystal is an indirect semiconductor with an optical band gap of 4.10 eV. After 980 nm laser excitation, the Ho^{3+} and Yb^{3+} co-doped $La_7P_3O_{18}$ phosphors show the characteristic blue (486 nm), green (550 nm), and red (661 nm) luminescence peaks of Ho^{3+} ions. The peak at 661 nm dominates in the up-conversion luminescence spectra of samples. Meanwhile, with the increase of Ho^{3+} and Yb^{3+} doping content, the up-conversion luminescence intensity increases first and then decreases. By increasing the doping contents of Ho^{3+} and Yb^{3+} up to 1 at.% and 10 at.%, respectively, concentration quenching may appear by an electric quadrupole−electric quadrupole interaction process. The pumping power dependence of luminescence indicates that the green and red emissions of samples are excited by a two-photon absorption process. The color coordinates of Ho^{3+} and Yb^{3+} co-doped $La_7P_3O_{18}$ crystals locate in the orange−red region.

Key words: $La_7P_3O_{18}$; Ho^{3+}; Yb^{3+}; up-conversion luminescence

1 Introduction

Rare earth-doped up-conversion luminescent materials have gained increasing attention in the last decade attributed to their enormous applications in solid-state lasers [1], sensors [2], biocatalyst [3], biolabeling [4], anti-counterfeiting [5], bioimaging [6], drug delivery [7], photodynamic therapy [8], solar energy [9], lighting and display [10], and information storage [11]. It is well known that both rare earth ions and host materials play key roles in determining the properties of rare earth doped luminescent materials [12]. Among the rare earth doped up-conversion luminescent materials, Ho^{3+} is one of the most frequently utilized ions due to its green/red up-converted emission band near 550/661 nm upon 980 nm laser pump [13]. However, Ho^{3+} single-doped up-conversion luminescent materials exhibit low-intensity emission due to the low absorption cross-section of Ho^{3+} around 980 nm. Fortunately, Yb^{3+} is often used for co-doping with Ho^{3+} as sensitizer ions to highly improve up-conversion luminescence properties of Ho^{3+} doped phosphors because of the peak absorption cross-section of Yb^{3+} near 980 nm and the ability of effective excitation energy transfer from Yb^{3+} to Ho^{3+} [14]. In addition, Yb^{3+} and Ho^{3+} co-doped

Corresponding author: Hai-bin LI, E-mail: coastllee@hotmail.com;
Jin-yu YANG, Tel: +86-851-83227341, E-mail: jinyuyang@gmail.com
DOI: 10.1016/S1003-6326(23)66176-X

up-conversion luminescent materials usually emit green light and are rarely used as red-emitting up-conversion luminescent materials, which makes the investigation of red-emitting Yb^{3+} and Ho^{3+} co-doped up-conversion luminescent materials very interesting and important.

It should be noted that the energy transfer rate from Yb^{3+} to Ho^{3+} is strongly dependent on the host matrix which has effects on the electronic transitions of 4f levels. So far, various materials have been proven as promising hosts for up-conversion phosphors such as halides [15], fluorides [5], sulfides [16], oxysulfides [17], oxyfluorides [18], ferroelectric oxides [19], rare earth oxides [20], rare earth phosphates [21], and so on. Among them, rare earth phosphates have gained attention as excellent host matrix candidates for rare earth phosphors attributed to their fabulous chemical and physical durability, low toxicity, and suitable rare earth ions accommodation [21]. As a member of the rare earth phosphate family, lanthanum oxophosphate ($La_7P_3O_{18}$) has received particular interest owing to the unique structure and excellent properties. Recently, some reports were published on the preparation, proton conductivity, and down-shifting luminescence properties of $La_7P_3O_{18}$ crystals. AMEZAWA et al [22] synthesized pure phase $La_7P_3O_{18}$ crystals and observed considerable proton conductivity in wet atmospheres. HATADA et al [23] successfully prepared $La_7P_3O_{18}$ crystals and discovered the dependence of the phase composition of samples on the calcination temperature. LIU and WANG [24] synthesized a polyphase Eu^{3+} doped $LaPO_4$–La_3PO_7–$La_7P_3O_{18}$ red phosphors by co-deposition and high-temperature solid-state method, and discussed the luminescence performance. However, to the best of our knowledge, few studies have been carried out on the up-conversion luminescence properties of $La_7P_3O_{18}$ phosphors.

In the present work, Ho^{3+} and Yb^{3+} co-doped $La_7P_3O_{18}$ phosphors were synthesized by a high-temperature solid-state process to obtain a red-emitting up-conversion luminescent material. The structure, optical, and up-conversion luminescence properties of the as-prepared phosphors were explored. The up-conversion luminescence mechanism and the concentration quenching mechanism of Ho^{3+} and Yb^{3+} co-doped $La_7P_3O_{18}$ crystals were also investigated.

2 Experimental

La_2O_3 (99.99%), Yb_2O_3 (99.99%), Ho_2O_3 (99.99%), and $NH_4H_2PO_4$ (AR) were purchased from the Aladdin Reagent Corporation. All the reagents in the research are of analytical grade and used as supplied without purification. In this study, a high-temperature solid-phase method was used to synthesize $La_7P_3O_{18}$ phosphors. A typical procedure is described as follows: first, 1.0720 g (3.290 mmol) La_2O_3, 0.0690 g (0.175 mmol) Yb_2O_3, 0.0132 g (0.035 mmol) Ho_2O_3, and 0.3450 g (3.000 mmol) $NH_4H_2PO_4$ are loaded into a 100 mL ball mill jar, and then 30 mL absolute ethanol was added as a dispersant. Afterward, the mixture was ball-milled at 4000 r/min at room temperature for 9 h and then dried at 70 ℃ for 50 min to obtain a precursor. Finally, the precursor was calcined at 1300 ℃ for 5 h in air to achieve the sample.

The phase structure of the prepared samples was measured using a Bruker D8 Advance X-ray diffractometer. The absorption spectrum of the synthesized phosphor was detected with a UV−2450 ultraviolet−visible spectrophotometer. The up-conversion photoluminescence (UPL) spectra were characterized by an FL−4600 fluorescence spectrometer with a 980 nm laser.

3 Results and discussion

3.1 Phase structures

Figure 1 depicts the XRD patterns for the $La_7P_3O_{18}$ samples with different Ho^{3+} doping amounts. As presented in Fig. 1, some prominent peaks, which are located at 2θ=12.027°, 25.165°, 26.984°, 28.399°, 29.208°, 30.168°, and 33.705°, can be assigned to $La_7P_3O_{18}$ (JCPDS No. 33-0719). Meanwhile, some slight diffraction peaks assigned to $LaPO_4$ (JCPDS No. 12-0283) can also be observed in all patterns, as denoted by diamond in Fig. 1. Moreover, no peaks related to other impurities are found in the XRD patterns, implying that Ho^{3+} and Yb^{3+} are ideally introduced into the $La_7P_3O_{18}$ crystal. These results reveal that all the samples are mixtures of monoclinic structure $La_7P_3O_{18}$ crystals with $P21/n$ space group [24] and minor monoclinic $LaPO_4$ crystals. It can be also found in the pattern that the half-height widths of diffraction peaks for the samples vary with the Ho^{3+}

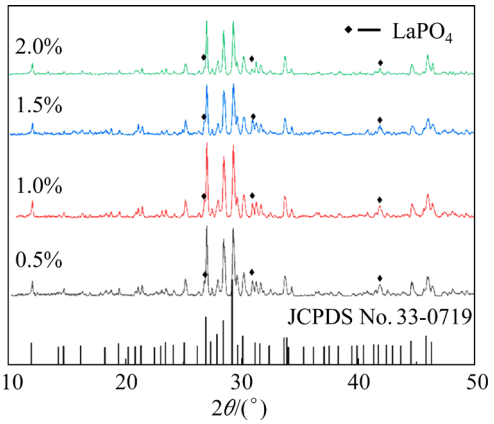

Fig. 1 XRD patterns of $La_7P_3O_{18}$ samples with different Ho^{3+} doping amounts (5 at.% Yb^{3+})

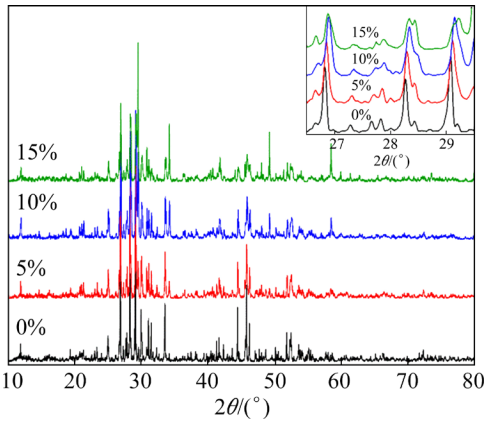

Fig. 2 XRD patterns of $La_7P_3O_{18}$ samples with different Yb^{3+} doping amounts (1 at.% Ho^{3+})

doping amounts. Taking the strongest diffraction peak at around 2θ=27.001° as an example, as the Ho^{3+} doping contents are 0.5, 1.0, 1.5, and 2.0 at.%, the half-height widths of the diffraction peak are (0.123±0.004)°, (0.102±0.003)°, (0.117±0.004)°, and (0.131±0.005)°, respectively, suggesting that the higher crystallinity of the sample with a Ho^{3+} doping content of 1% than that of the other samples.

The XRD patterns of the $La_7P_3O_{18}$ samples with different Yb^{3+} doping amounts are described in Fig. 2. As shown in Fig. 2, all samples display similar XRD patterns to those in Fig. 1, revealing that the as-obtained products are mixtures of $La_7P_3O_{18}$ crystals and minor $LaPO_4$ crystals. It should be noted that the intensities of the diffraction peaks of samples are found to change with increasing Yb^{3+} doping amount. The intensities of the $(\bar{4}31)$, $(\bar{1}24)$, and (232) peaks, which located at around 2θ=26.77°, 28.19°, and 29.04°, respectively, decrease. However, the intensity of the $(\bar{5}32)$ peak at about 2θ=29.52° increases. This means that the Yb^{3+} doping level affects the growth orientation of the samples. In addition, the peaks of samples shift to a high degree with the rise of Yb^{3+} doping amount, as illustrated in the inset in Fig. 2. The reason is that the ionic radium of Ho^{3+} and Yb^{3+} is smaller than that of La^{3+}. The more the amounts of Yb^{3+} and Ho^{3+} ions are doped into the $La_7P_3O_{18}$ lattice (Yb and Ho replacing the La site), the smaller the unit cell parameters of samples are, and the more the diffraction peaks shift toward the larger angles [25]. The above results imply that Ho^{3+} and Yb^{3+} ions successfully enter the $La_7P_3O_{18}$ matrix lattice by occupying La^{3+} sites.

3.2 UV−visible diffuse reflectance spectrum of $La_7P_3O_{18}$: 2% Ho^{3+}, 5% Yb^{3+}

The UV−visible diffuse reflectance spectrum (UV−Vis DRS) of the representative $La_7P_3O_{18}$: 2% Ho^{3+}, 5% Yb^{3+} is presented in Fig. 3(a). As exhibited in Fig. 3(a), the sample shows a strong absorption in UV range with an adsorption edge at about 290 nm. The optical band gap is determined by the following equation [26]:

$$\alpha h\upsilon = B(h\upsilon - E_g)^{\gamma} \quad (1)$$

where α is the absorption coefficient, B is an appropriate constant, $h\upsilon$ is the energy of the incident photon, E_g is the optical band gap, and γ is a constant which characterizes the electronic transition of the optical absorption. Theoretically, γ decides the transition characteristics of a semiconductor (γ=1/2 for direct transition or γ=2 for indirect transition). As shown in the inset in

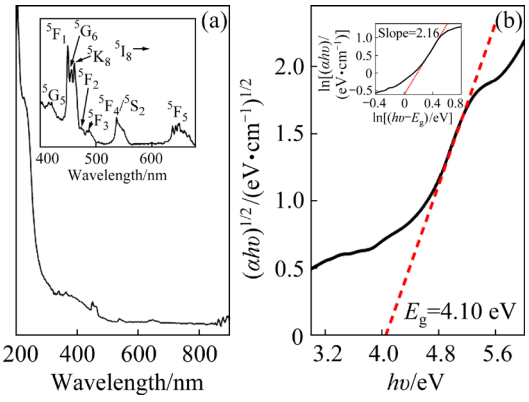

Fig. 3 UV−visible diffuse reflectance spectrum of $La_7P_3O_{18}$: 2% Ho^{3+}, 5% Yb^{3+} (inset shows zoom in range of 400−680 nm) (a); Curve of $(\alpha h\upsilon)^{1/2}$ versus $h\upsilon$ (inset shows curve of $\ln(\alpha h\upsilon)$ vs $\ln(h\upsilon - E_g)$) (b)

Fig. 3(b), the slope of ln($\alpha h\upsilon$) against ln($h\upsilon - E_g$) is about 2.16, indicating that $La_7P_3O_{18}$ is an indirect semiconductor and γ should be 2 [26]. The plot of $(\alpha h\upsilon)^{1/2}$ versus photon energy ($h\upsilon$) is shown in Fig. 3(b), from which the optical band gap of $La_7P_3O_{18}$ is estimated to be 4.10 eV [27]. Additionally, some small absorption bands at 400−680 nm (the inset of Fig. 3(a)) appear due to the Ho^{3+} doped in the $La_7P_3O_{18}$ crystals. The weak absorption bands located at about 418, 449, 455, 461, 473, 486, 539, and 650 nm correspond to the electronic transitions of Ho^{3+} from the ground level $^5I_8$ to $^5G_5$, $^5F_1$, $^5G_6$, $^5K_8$, $^5F_2$, $^5F_3$, $^5F_4/^5S_2$, and $^5F_5$, respectively, which are consistent with the previous reports [28], indicating that Ho^{3+} is successfully doped into the $La_7P_3O_{18}$ matrix.

3.3 Up-conversion luminescence properties of Ho^{3+} and Yb^{3+} co-doped $La_7P_3O_{18}$ crystals

Figures 4 and 5 show the up-conversion luminescence spectra of Ho^{3+} and Yb^{3+} co-doped $La_7P_3O_{18}$ samples with different doping amounts excited by a 980 nm laser. The results show that the up-conversion emission spectra of the Ho^{3+} and Yb^{3+} co-doped $La_7P_3O_{18}$ samples are constituted by some similar emission bands under the excitation of 980 nm. The three emission bands located at 486, 550, and 661 nm can be observed, attributing to the $^5F_3 \rightarrow {}^5I_8$, $^5S_2/^5F_4 \rightarrow {}^5I_8$, and $^5F_5 \rightarrow {}^5I_8$ transitions of Ho^{3+} ions, respectively [29]. Meanwhile, the intensities of the peaks at 550 and 661 nm are much stronger than those at 486 nm. Interestingly, the red emission peak at 661 nm dominates the emission spectra of samples, while in general the most substantial up-conversion emission peak is located

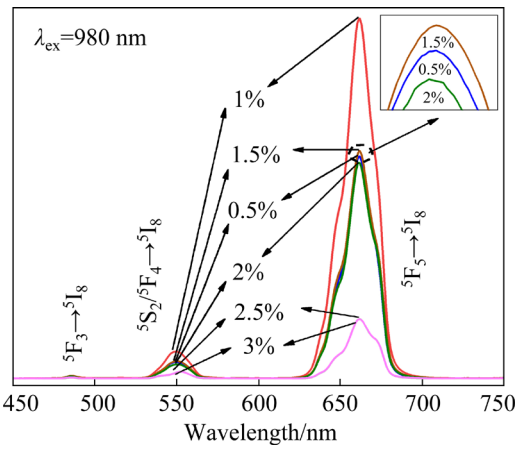

Fig. 4 Up-conversion emission spectra of $La_7P_3O_{18}$: x% Ho^{3+}, 5% Yb^{3+} (x=0.5, 1, 1.5, 2, 2.5, 3) samples

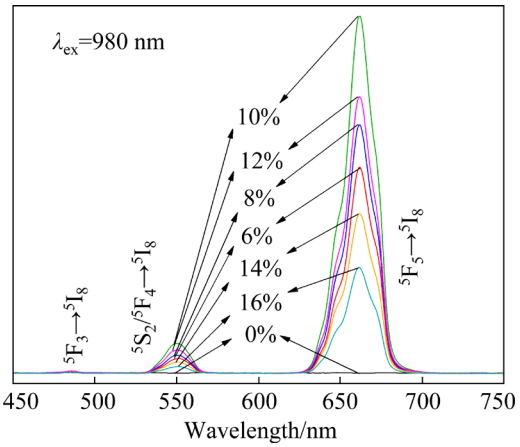

Fig. 5 Up-conversion emission spectra of $La_7P_3O_{18}$: 1% Ho^{3+}, y% Yb^{3+} (y=0, 6, 8, 10, 12, 14, 16) samples

in the green region for the Ho^{3+} and Yb^{3+} co-doped materials such as halides [15], ferroelectric oxides [19], and rare earth oxides [20]. This may be attributed to the unique crystal structure of the $La_7P_3O_{18}$ matrix.

It can also be seen from Fig. 4 that the up-conversion luminescence intensity of the sample varies with the doping amount of Ho^{3+}, but the positions of the up-conversion luminescence peaks are almost the same. As the Ho^{3+} doping level increases, the intensity of luminescence increases initially and then decreases, reaching the maximum when the Ho^{3+} doping content is 1%, suggesting that concentration quenching happens if the Ho^{3+} doping content is above 1%. As mentioned above, Ho^{3+} ions play a role as activators in $La_7P_3O_{18}$ to emit light as irradiated by 980 nm laser with the help of Yb^{3+}. When the doping of Yb^{3+} is controlled at a level amount, increasing the doping amount of Ho^{3+} in $La_7P_3O_{18}$ will result in both positive and negative effects for luminescence. On the one hand, higher doping amount of Ho^{3+} means more activators in $La_7P_3O_{18}$, which leads to a higher luminescence intensity. On the other hand, increasing doping amount of Ho^{3+} means reducing the distances between Ho^{3+} ions in $La_7P_3O_{18}$, which raises the probability of non-radiative cross-relaxation among Ho^{3+} ions to decrease the luminescence intensity. When the doping level of Ho^{3+} exceeds 1%, the dominant role of the positive effect is replaced by the negative effect, thus the decrease of luminescence intensity and the occurrence of concentration quenching [30].

Figure 5 shows the up-conversion emission

spectra of $La_7P_3O_{18}$: 1% Ho^{3+}, y% Yb^{3+} samples with different Yb^{3+} doping levels. It is illustrated that the up-conversion luminescence intensities increase first with the increase of Yb^{3+} doping amount and reach the maximum value at 10%, and then decrease accordingly. The decrease of the emission intensity at high Yb^{3+} doping level may be explained by concentration quenching attributed to the fact that the energy transfer rate among rare earth ions is inversely proportional to the sixth power of the distance between donors and acceptors [31]. When the Yb^{3+} doping amount is controlled below 10%, the relatively higher Yb^{3+} content in the $La_7P_3O_{18}$ allows more energy transfer from Yb^{3+} to Ho^{3+}, which enhances the up-conversion luminescence intensity. As the Yb^{3+} doping amount is raised above 10%, the distance between rare earth ions reduces, leading to the increase of the rate of energy back transfer (EBT) from Ho^{3+} to Yb^{3+} [32] and the probability of non-radiative energy transfer [33] among Yb^{3+} ions, thus the decrease of the up-conversion luminescence intensity.

Generally, there are three possible mechanisms for concentration quenching, including radiation reabsorption, energy transfer, and electric multipole interaction [34]. Radiation reabsorption mechanism can be ruled out because the fluorescence spectra do not overlap, as shown in Fig. 4 and Fig. 5 [35]. The critical distance (R_C) for energy transfer between activators can be calculated as follows [36]:

$$R_C = 2\sqrt[3]{\frac{3V}{4\pi N x_c}} \tag{2}$$

where V is the unit cell volume, x_c is the critical quenching concentration, and N is the number of $La_7P_3O_{18}$ molecule units in the unit cell. For $La_7P_3O_{18}$, V is 3585.03 Å^3, x_c is 0.01, and N is 4. The calculated R_C is 55.53 Å, which is far greater than the critical distance (5 Å) for energy transfer. So, the energy transfer mechanism is also excluded, indicating that the concentration quenching mechanism for the prepared sample can only be the electric multipole interaction. In order to confirm this point, the electric multipole interaction effect is analyzed. van UITERT [37] suggests that the relationship between doping concentration and integrated luminescence intensity follows

$$\left(\frac{I}{x(y)}\right) = K\{1+\beta[x(y)]^{Q/3}\}^{-1} \tag{3}$$

where I is integrated luminescence intensity; $x(y)$ is doping content; K and β are constants for a particular host under fixed excitation conditions; Q is the electric multipole interaction parameter that takes values of 6, 8, and 10 for electric dipole−electric dipole interaction (d−d), electric dipole−electric quadrupole interaction (d−p), and electric quadrupole−electric quadrupole interaction (p−p), respectively [37]. According to the above equation, the value of $-Q/3$ can be estimated as the slope of $\lg(I/x)$ versus $\lg x$ plot.

Figure 6 illustrates the plot of $\lg(I/x)$ against $\lg x$ for the $La_7P_3O_{18}$: x% Ho^{3+}, 5% Yb^{3+} samples. It can be seen that the slope of the fitting line is −2.76. So, the Q is found to be approximately 8, confirming that the concentration quenching mechanism of Ho^{3+} up-conversion emission is the electric dipole−electric quadrupole interaction.

Similarly, the plot of $\lg(I/y)$ against $\lg y$ is also applied for the $La_7P_3O_{18}$: 1% Ho^{3+}, y% Yb^{3+} samples, as shown in Fig. 7. The slope of the fitting

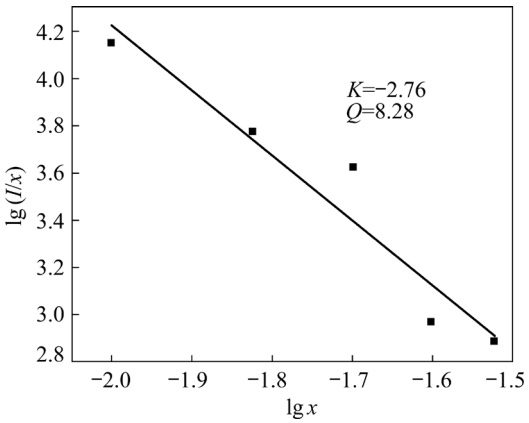

Fig. 6 Plot of $\lg(I/x)$ against $\lg x$ for $La_7P_3O_{18}$: x% Ho^{3+}, 5% Yb^{3+} samples

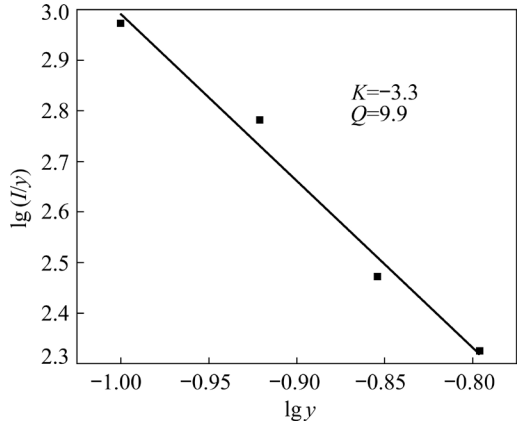

Fig. 7 Plot of $\lg(I/y)$ against $\lg y$ for $La_7P_3O_{18}$: 1% Ho^{3+}, y% Yb^{3+} samples

line is −3.3, so the corresponding Q is close to 10, revealing that the concentration quenching mechanism of Ho^{3+} and Yb^{3+} co-doping in the $La_7P_3O_{18}$ sample is dominated by electric quadrupole−electric quadrupole interaction.

Figure 8 illustrates the up-conversion emission spectra of $La_7P_3O_{18}$: 1% Ho^{3+}, 10% Yb^{3+} excited at different pump powers. It can be observed that the up-conversion luminescence intensity of the sample gradually increases with rising pump power from 0.55 to 3.45 W. The relation between up-conversion luminescence intensity and pumping power can be described by the following formula:

$$I \propto P^n \tag{4}$$

where P is pumping power, and the index n is the number of near-infrared photons required for the up-conversion luminescence process that can be measured as the slope of lg I versus lg P plot [38]. The double-logarithmic plots of the integrated up-conversion luminescence intensities of green and red emission bands and pumping power are shown in Fig. 9. It can be ascertained that the slopes for the green band at 550 nm and the red emission at 661 nm are 1.71 and 1.43, respectively, indicating that the $^5S_2/^5F_4 \rightarrow {}^5I_8$ energy level transition at 550 nm and the $^5F_5 \rightarrow {}^5I_8$ energy level transition at 661 nm are both two-photon absorption process as the calculated n-values are close to 2. The reason why the index n for green and red emission bands is greater than 1 and less than 2 may be ascribed to the decrease of the up-conversion emission intensity, which is resulted from the non-radiative transitions in the sample and the thermal effects caused by the strong absorption of the sample [39].

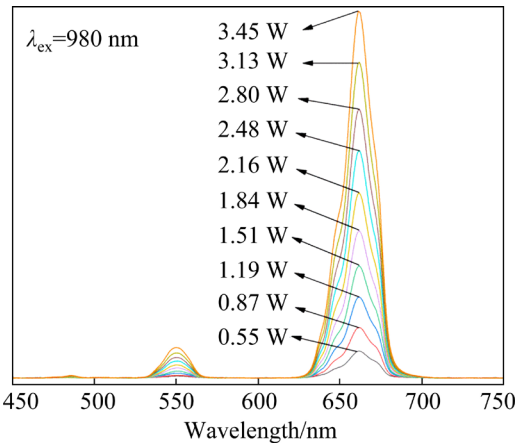

Fig. 8 Up-conversion emission spectra of $La_7P_3O_{18}$: 1% Ho^{3+}, 10% Yb^{3+} excited by different pumping powers

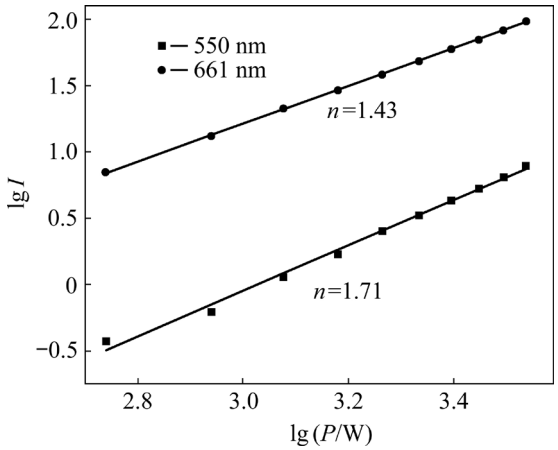

Fig. 9 Relationships of lg I vs lg P with linear fittings for green and red emission bands of $La_7P_3O_{18}$: 1% Ho^{3+}, 10% Yb^{3+}

A possible energy transfer process for the up-conversion luminescence mechanism for $La_7P_3O_{18}$: 1% Ho^{3+}, 10% Yb^{3+} sample is schematically depicted in Fig. 10. It can be seen that there is not level of Ho^{3+} ion matching the energy of 980 nm near-infrared photons, which means that the absorption of the photons of 980 nm by Ho^{3+} ions may not happen. In contrast, the excited $^2F_{5/2}$ level of Yb^{3+} ion is consistent with the energy of 980 nm photons, suggesting that the Yb^{3+} ion can easily absorb the photons of 980 nm laser and then be used as effective sensitizers to transfer absorbed energy to Ho^{3+} ions for the up-conversion process. As for the Yb^{3+} and Ho^{3+} co-doped $La_7P_3O_{18}$ crystals, many valence electrons of Yb^{3+} are populated to the $^2F_{5/2}$ level via a ground state absorption (GSA) process induced by 980 nm laser excitation. Some excited electrons decay to the ground state, while some transfer the excitation energy to Ho^{3+} ions to undergo an energy transfer (ET1) process to promote the valence electrons of Ho^{3+} to the $^5I_6$ level. A part of the $^5I_6$ level electrons of Ho^{3+} may relax non-radiatively to the $^5I_7$ level, and then be excited into the $^5F_5$ level through an excited state absorption (ESA1) process due to the excitation of 980 nm laser, followed by the decay to the ground state $^5I_8$ radiating 661 nm red light. Meanwhile, another part of excited $^5I_6$ level electrons of Ho^{3+} can be further promoted to the $^5S_2/^5F_4$ state via an excited state absorption (ESA2) process induced by 980 nm laser excitation or an energy transfer (ET2) process from excited electrons of Yb^{3+} ions. The $^5S_2/^5F_4$ level electrons

then relax radiatively to the $^5I_8$ state emitting photons in green light (550 nm). It should be noted that some electrons in the $^5S_2/^5F_4$ level may decay non-radiatively to the $^5F_5$ level followed by radiative relaxing to the ground state, $^5I_8$, which may lead to the emission of red light at 661 nm. In addition, a few $^5F_5$ level electrons can be excited to the $^5F_3$ level by a cross-relaxation (CR) process, $^5F_5 + {}^5I_7 \rightarrow {}^5F_3 + {}^5I_8$, and then decay to the ground state and radiate a weak blue ($^5F_3 \rightarrow {}^5I_8$) up-conversion emission at 486 nm [40].

Figure 11 shows the calculated coordinates for the $La_7P_3O_{18}$: x% Ho^{3+}, 10% Yb^{3+} samples with different Ho^{3+} doping contents in the CIE chromaticity diagram. It can be seen that the up-conversion emissions of the $La_7P_3O_{18}$: x% Ho^{3+}, 10% Yb^{3+} samples all locate in the orange-red region. By taking $La_7P_3O_{18}$: 1% Ho^{3+}, 10% Yb^{3+} for example, the calculated color coordinate is (0.6167, 0.3757). The CIE coordinate calculation results indicate that the $La_7P_3O_{18}$: x% Ho^{3+}, 10% Yb^{3+} crystals are potential orange−red up-conversion luminescent materials.

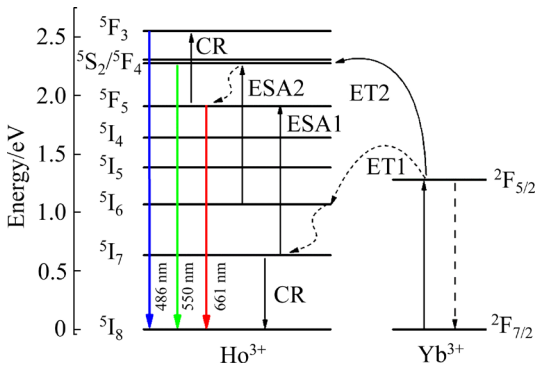

Fig. 10 Schematic diagram of possible up-conversion luminescence mechanism for $La_7P_3O_{18}$: 1% Ho^{3+}, 10% Yb^{3+}

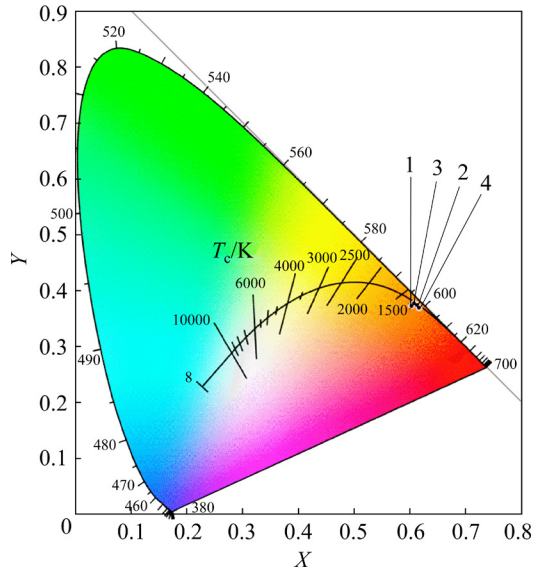

Fig. 11 CIE chromaticity diagram for $La_7P_3O_{18}$: x% Ho^{3+}, 10% Yb^{3+} samples (1—x=0.5; 2—x=1; 3—x=1.5; 4—x=2)

4 Conclusions

(1) A series of Ho^{3+}/Yb^{3+} co-doped $La_7P_3O_{18}$ up-conversion phosphors were synthesized using a high-temperature solid-state reaction at 1300 ℃. XRD patterns reveal that the as-prepared samples are mixtures of monoclinic $La_7P_3O_{18}$ crystals and minor monoclinic $LaPO_4$ crystals.

(2) UV−Vis DRS results indicate that $La_7P_3O_{18}$ crystal is an indirect semiconductor with an optical band gap value of 4.10 eV.

(3) Under the excitation of 980 nm near-infrared light, the Ho^{3+}/Yb^{3+} co-doped $La_7P_3O_{18}$ phosphors show the characteristic blue, green, and red up-conversion emission of Ho^{3+} ions at 486 nm ($^5F_3$–$^5I_8$), 550 nm ($^5F_4/^5S_2$–$^5I_8$), and 661 nm ($^5F_5$–$^5I_8$), respectively. The red emission band at 661 nm dominates the up-conversion luminescence spectra of samples. The calculated coordinates of samples all locate in the orange−red region.

(4) With the increase of Ho^{3+} and Yb^{3+} doping levels, the up-conversion luminescence intensity increases at first and then decreases. With increasing the doping contents of Ho^{3+} and Yb^{3+} up to 1% and 10%, respectively, concentration quenching appears due to the electric quadrupole−electric quadrupole interaction.

(5) The pumping power dependence of up-conversion luminescence indicates that the 550 nm and 661 nm up-conversion emissions of Ho^{3+} and Yb^{3+} co-doped $La_7P_3O_{18}$ phosphors are attributed to a two-photon absorption process.

Acknowledgments

This work was supported by Guizhou Provincial Science and Technology Foundation, China (No. [2019]1229), and the National Natural Science Foundation of China (Nos. 21361007, 51776046).

References

[1] ANGLE F B, YAO Kai-yuan, BARNARD E S, BORYS N J, LEVW E S, TIAN Bi-ning, TAJION C A, LUCA M,

VIRGINIA ALTOE M, SHAUL A, KENES B, FRANCESCO S, COHEN B E, CHAN E M, JAMES SCHUCK P. Continuous-wave upconverting nanoparticle microlasers [J]. Nature Nanotechnology, 2018, 13: 572−577.

[2] ZHANG Zhi-yu, JIN Min-kun, YAO Le-yi, GUO Chong-feng. NIR dual-mode temperature sensor based on FIR technology in $BaYF_5$: Nd^{3+}/Yb^{3+} [J]. Optical Materials, 2021, 121: 111607.

[3] WANG Zhao, LIU Bin, SUN Qian-qian, FENG Li-li, HE Fei, YANG Piao-ping, GAI Shi-li, QUAN Ze-wei, LIN Jun. Upconverted metal-organic framework Janus architecture for near-infrared and ultrasound co-enhanced high performance tumor therapy [J]. ACS Nano, 2021, 15(7): 12342−12357.

[4] CHEN Hong-qi, TANG Wei, LIU Yun-chun, WANG Lun. Quantitative image analysis method for detection of nitrite with cyanine dye-$NaYF_4$: Yb, Tm@ $NaYF_4$ upconversion nanoparticles composite luminescent probe [J]. Food Chemistry, 2022, 367: 130660.

[5] CHEN Yin, XIE Shao-wen, TONG Chao, TAN Hai-hu, XU Li-jian, LI Na, XU Jian-xiong. Preparation of $NaYF_4$: Yb^{3+}, Tm^{3+}@ $NaGdF_4$: Ce^{3+}, Eu^{3+} double-jacket microtubes for dual-mode fluorescent anti-counterfeiting [J]. Transactions of Nonferrous Metals Society of China, 2020, 30(12): 3333−3346.

[6] YANG Dong-peng, CAO Cong, FENG Wei, HUANG Chun-hui, LI Fu-you. Synthesis of $NaYF_4$: Nd@ $NaLuF_4$@ SiO_2@ PS colloids for fluorescence imaging in the second biological window [J]. Journal of Rare Earths, 2018, 36(2): 113−118.

[7] ZHANG Zhen, JAYAKUMAR M K G, SHIKHA S, ZHANG Yi, ZHENG Xiang, ZHANG Yong. Modularly assembled upconversion nanoparticles for orthogonally controlled cell imaging and drug delivery [J]. ACS Applied Materials & Interfaces, 2020, 12(11): 12549−12556.

[8] MOKOENA P P, OLUWOLE D O, NYOKONG T, SWART H C, NTWAEABORWA O M. Enhanced upconversion emission of Er^{3+}−Yb^{3+} co-doped $Ba_5(PO_4)_3OH$ powder phosphor for application in photodynamic therapy [J]. Sensors and Actuators A: Physical, 2021, 331: 113014.

[9] QIAO Yu, LI Shu-han, LIU Wen-hui, RAN Mei-qing, LU Hai-fei, YANG Ying-ping. Recent advances of rare-earth ion doped luminescent nanomaterials in perovskite solar cells [J]. Nanomaterials, 2018, 8(1): 43−47.

[10] DONG Hao, SUN Ling-dong, YAN Chun-hua. Local structure engineering in lanthanide-doped nanocrystals for tunable upconversion emissions [J]. Journal of the American Chemical Society, 2021, 143(49): 20546−20561.

[11] BAI Xue, CUN Yang-ke, XU Zan, ZI Ying-zhu, HAIDER A A, ULLAH A, KHAN I, QIU Jian-bei, SONG Zhi-guo, YANG Zheng-wen. Multiple anti-counterfeiting and optical storage of reversible dual-mode luminescence modification in photochromic $CaWO_4$: Yb^{3+}, Er^{3+}, Bi^{3+} phosphor [J]. Chemical Engineering Journal, 2022, 429: 132333.

[12] ZHANG Xiang-yu, WANG Dan, SHI Huan-wen, WANG Jin-guo, HOU Zhao-yang, ZHANG Li-dong, GAO Dang-li. Effect of host matrix on Yb^{3+} concentration controlled red to green luminescence ratio [J]. Acta Physica Sinica, 2018, 67(8): 084203.

[13] CHO H, HWANG S M, LEE J B, KA D H, KIM T W, LEE B S, LEE J Y, LEE J I, RYU J H. White luminescence of $Ho^{3+}/Tm^{3+}/Yb^{3+}$-codoped $CaWO_4$ synthesized via citrate complex route assisted by microwave irradiation [J]. Transactions of Nonferrous Metals Society of China, 2014, 24(S1): s134−s140.

[14] WANG Xin-yu, ZHANG Chao-yi, HU Dai, LI Wen-bo, LIN Hai, ZENG Fan-ming, LI Chun, SU Zhong-min. Influence of Yb ions concentration on Ho: BaY_2F_8 crystals emission in the range of 1−3 μm [J]. Optical Materials, 2020, 109: 110141.

[15] PRZYBYLSKA D, EKNER-GRZYB A, GRZEŚKOWIAK B F, GRZYB T. Upconverting SrF_2 nanoparticles doped with Yb^{3+}/Ho^{3+}, Yb^{3+}/Er^{3+} and Yb^{3+}/Tm^{3+} ions−Optimisation of synthesis method, structural, spectroscopic and cytotoxicity studies [J]. Scientific Reports, 2019, 9: 8669.

[16] GUPTA I, SINGH S, BHAGWAN S, SINGH D. Rare earth (RE) doped phosphors and their emerging applications: A review [J]. Ceramics International, 2021, 47: 19282−19303.

[17] ALEKSANDER Ć, MILICA S, KEVIL S, BISHWAJIT S C, MIROSLAV D D. Upconversion photoluminescence of sub-micron lanthanum oxysulfide particles co-doped with Yb^{3+}/Ho^{3+} and Yb^{3+}/Tm^{3+} synthesized by optimized combustion technique [J]. Optical Materials, 2021, 120: 111417.

[18] TIAN Ying, LIU Qun-huo, E Fei, YE Ren-guang, CHEN Shu-ting, ZHANG Jun-jie, XU Shi-qing. Structural evolution, crystallization behaviour and mid-infrared emission properties in Yb/Ho codoped oxyfluoride germanosilicate glass ceramics with varied Si/Ge ratio [J]. Infrared Physics & Technology, 2021, 116: 103741.

[19] LU Zi-han, LI Kai-xuan, WANG Jun, LUO Lai-hui. Photochromic and temperature sensing properties of Ho^{3+}−Yb^{3+} codoped $Bi_{0.495-x}Na_{0.5}TiO_3$ ceramics [J]. Optical Materials, 2021, 111: 110718.

[20] XIANG Guo-tao, MA Yan, LIU Wen, JIANG Sha, LUO Xiao-bing, LI Li, ZHOU Xian-ju, GU Zhi-wei, WANG Jia-peng, LUO Yong-shi, ZHANG Jia-hua. Improvement of green upconversion monochromaticity by doping Eu^{3+} in Lu_2O_3:Yb^{3+}/Ho^{3+} powders with detailed investigation of the energy transfer mechanism [J]. Inorganic Chemistry, 2017, 56(15): 9194−9199.

[21] RIVERA S I, CARRILLO F J, GARCIA A, OLIVA J. Up-conversion of luminescence in YPO_4: Er^{3+} powders: A new technique [J]. Materials Letters, 2017, 187: 83−85.

[22] AMEZAWA K, TOMII Y, YAMAMOTO N. High-temperature protonic conduction in $La_7P_3O_{18}$ [J]. Solid State Ionics, 2004, 175(1/2/3/4): 569−573.

[23] HATADA N, NAGAI T, NOSE Y, UDA T. Reinvestigation of the phase equilibria in the La_2O_3−P_2O_5 system [J]. Journal of Phase Equilibria and Diffusion, 2013, 34(3): 196−201.

[24] LIU Ru, WANG Xi-gui. Luminescence properties of a novel red phosphor $6LaPO_4$−$3La_3PO_7$−$2La_7P_3O_{18}$:Eu^{3+} [J]. Luminescence, 2020, 35(1): 114−119.

[25] LIU Shui-fu, LIU Song-bin, MING Hong, HOU Dejian, YOU Wei-xiong, Ye Xin-yu. Investigation on the upconversion luminescence in Ho^{3+}/Yb^{3+} co-doped $Ba_3Sc_4O_9$ phosphor [J]. Materials Research Bulletin, 2018, 98: 187−193.

[26] DAVIS E A, MOTT N F. Conduction in non-crystalline

systems V: Conductivity, optical absorption and photoconductivity in amorphous semiconductors [J]. The Philosophical Magazine: A Journal of Theoretical Experimental and Applied Physics, 1970, 22(179): 903−922.

[27] TAUC J, GRIGOROVICI R, VANCU A. Optical properties and electronic structure of amorphous germanium [J]. Physica Status Solidi, 1966, 15(2): 627−637.

[28] ZHOU You-shi, CHEN Jun-xian, DONG Liang, CAO Shu-xuan, ZHANG Yu-xia, HAN Wen-juan, XU Hong-hao, LIU Jun-hai. Growth and spectroscopic properties of Yb−Ho co-doped CNGG crystal [J]. Optical Materials, 2021, 114: 110998.

[29] MONIKA, YADAV R S, RAI A R, RAI S B. NIR light guided enhanced photoluminescence and temperature sensing in $Ho^{3+}/Yb^{3+}/Bi^{3+}$ co-doped $ZnGa_2O_4$ phosphor [J]. Scientific Reports, 2021, 11: 4148.

[30] LI Ting, GUO Chong-feng, YANG Yan-min, LI Lin, ZHANG Ning. Efficient green up-conversion emission in Yb^{3+}/Ho^{3+} co-doped $CaIn_2O_4$ [J]. Acta Materialia, 2013, 61(19): 7481−7487.

[31] LOU Jin-hui, TANG Xiao-fang, ZHANG Hao-ke, GUAN Wei-jiang, LU Chao. Chemiluminescence resonance energy transfer efficiency and donor–acceptor distance: From qualitative to quantitative [J]. Angewandte Chemie International Edition, 2021, 60(23): 13029−13034.

[32] SUO Hao, GUO Chong-feng, WANG Wen-bin, LI Ting, DUAN Chang-kui, YIN Min. Mechanism and stability of spectrally pure green up-conversion emission in Yb^{3+}/Ho^{3+} co-doped $Ba_5Gd_8Zn_4O_{21}$ phosphors [J]. Dalton Transactions, 2016, 45(6): 2629−2636.

[33] NETO A N C, MOURA JR R T, MALTA O L. On the mechanisms of non-radiative energy transfer between lanthanide ions: Centrosymmetric systems [J]. Journal of Luminescence, 2019, 210: 342−347.

[34] FENG Hong-wei, XU Hui, FENG Hong-tu, GAO Ying, CHEN Xin, JIN Xin-yuan. Tuning photoluminescence in the Ce^{3+}/Tb^{3+} doped $Ca_2MgSi_2O_7$ phosphors [J]. Optik, 2019, 193: 162967.

[35] WANG Chuang, JIANG Jing, WANG Jian-rui, XIN Shuang-yu, SHI Yu-rong, ZHU Ge. Novel high color purity phosphors $Sr_9Mg_{1.5}(PO_4)_7$: Sm^{3+}, R^+ (R=Li, Na, K): Crystal structure, luminescence and thermal quenching property investigation [J]. Journal of Luminescence, 2019, 215: 116606.

[36] BLASSE G. Energy transfer in oxidic phosphors [J]. Physics Letters A, 1968, 28(6): 444−445.

[37] van UITERT L G. Characterization of energy transfer interactions between rare earth ions [J]. Journal of the Electrochemical Society, 1967, 114(10): 1048−1053.

[38] LI Fang-min, LIN Li, GUO Chong-feng, LI Ting, NOH H. M., JEONG J H. Up-conversion luminescence properties of Yb^{3+}–Ho^{3+} co-doped $CaLa_2ZnO_5$ [J]. Ceramics International, 2014, 40: 7363−7366.

[39] WANG Yan-ze, CHEN Bing, WANG Feng. Overcoming thermal quenching in upconversion nanoparticles [J]. Nanoscale, 2021, 13(6): 3454−3462.

[40] ZHAO Tian-li, WANG Si-ying, ZOU Xiang-yu, ZHANG Hong-bo, YAO Yi-meng, HUO Hong-hong, WANG Qian-wen, SU Chun-hui. Synthesis and up-conversion luminescence properties of Ho^{3+}–Yb^{3+} co-doped glass ceramics containing $Sr_3Gd(PO_4)_3$ [J]. Optical Materials, 2021, 121: 111547.

Ho^{3+}和 Yb^{3+}共掺杂 $La_7P_3O_{18}$荧光粉的合成及上转换发光性能

朱浩天[1]，郭海瑞[1]，郑启泾[1]，官春艳[1]，朱莉萍[2]，李海斌[3]，杨锦瑜[1]

1. 贵州师范大学 化学与材料科学学院 贵州省功能材料化学重点实验室，贵阳 550001；

2. 贵州师范大学 教育学院，贵阳 550001；

3. 玉林师范学院 化学与食品科学学院 广西农产资源化学与生物技术重点实验室，玉林 537000

摘 要：通过高温固相技术合成 Ho^{3+}和 Yb^{3+}共掺杂 $La_7P_3O_{18}$上转换荧光粉。XRD 结果表明，合成样品是空间群为 *P*21/*n* 的单斜结构的 $La_7P_3O_{18}$晶体和少量 $LaPO_4$晶体的混合物。紫外可见漫反射光谱结果证实 $La_7P_3O_{18}$晶体是一种光学带隙为 4.10 eV 的间接半导体。经 980 nm 激光激发，Ho^{3+}和 Yb^{3+}共掺杂 $La_7P_3O_{18}$荧光粉发射出 Ho^{3+}离子特征的蓝色(486 nm)、绿色(550 nm)和红色(661 nm)特征峰，其中，661 nm 处发射峰在样品上转换发光光谱中占主导地位。此外，随着 Ho^{3+}和 Yb^{3+}掺杂量的增加，样品上转换发光强度先增大后减小。当 Ho^{3+}和 Yb^{3+}的掺杂量分别达到 1%和 10%(摩尔分数)时，样品出现浓度猝灭现象，其机制为电四极−电四极相互作用。泵浦功率和发光强度关系表明，样品的绿光和红光发射均源于双光子吸收过程激发。Ho^{3+}和 Yb^{3+}共掺杂 $La_7P_3O_{18}$晶体上转换发光色坐标位于橙红色区域。

关键词：$La_7P_3O_{18}$；Ho^{3+}；Yb^{3+}；上转换发光

(Edited by Bing YANG)